Mapping the stray fields of a micromagnet using spin centers in SiC

Bejarano, M.; Trindade Goncalves, F. J.; Hollenbach, M.; Hache, T.; Hula, T.; Berencen, Y.; Faßbender, J.; Helm, M.; Astakhov, G.; Schultheiß, H.;

Originally published:

March 2021

IEEE Magnetics Letters 12(2021), 9380379

DOI: https://doi.org/10.1109/LMAG.2021.3066341

Perma-Link to Publication Repository of HZDR:

https://www.hzdr.de/publications/Publ-31418

Mapping the stray fields of a micromagnet using spin centers in SiC

Mauricio Bejarano[1], Francisco J. T. Goncalves[1], Michael Hollenbach[1,2], Toni Hache[1,3], Tobias Hula[1,3], Y. Berencén[1], Jürgen Fassbender[1], Manfred Helm[1], Georgy V. Astakhov[1], and Helmut Schultheiss[1]
[1]Helmholtz-Zentrum Dresden-Rossendorf, Institute of Ion Beam Physics and Materials Research, Bautzner Landstrasse 400, 01328 Dresden, Germany
[2]Technische Universität Dresden, 01062 Dresden, Germany
[3]Institut für Physik, Technische Universität Chemnitz, 09107 Chemnitz, Germany

Abstract **We report the use of optically addressable spin centers in SiC to probe the static magnetic stray fields generated by a ferromagnetic microstructure lithographically patterned on the surface of a SiC crystal. The stray fields cause shifts in the resonance frequency of the spin centers. The spin resonance in the spin centers is driven by a micrometer-sized microwave antenna patterned adjacent to the magnetic element. The patterning of the antenna is done to ensure that the driving microwave fields are delivered locally and more efficiently compared to conventional, millimeter-sized circuits. A clear difference in the resonance frequency of the spin centers in SiC is observed at various distances to the magnetic element, for two different magnetic states. Our results are a first step toward developing magnon-quantum applications by deploying the local microwave fields and the stray fields at the micrometer lengthscale.**

***Index Terms*—Magnetic Sensors, Optically Detected Magnetic Resonance, Spin centers in SiC, Magnetic dipolar fields.**

I. Introduction

Optically active vacancy-related qubits, among others, the nitrogen-vacancy (NV) center in diamond and the silicon-vacancy (V_{Si}) center in silicon carbide (SiC), are considered as nano-scale magnetic field sensors [1], [2] due to their long spin coherence time even at room temperature [3], [4]. A hybrid quantum platform consisting of such spin qubits and nanostructured magnetic circuits can bring new functionalities and analytics tools [5], [6]. By using state-of-the-art lithography techniques, magnetic nanostructures can be tailored such that the resulting magnetic dipolar field landscape locally affects the spin qubits. While isolated nanostructures act locally, they can also be built into periodic patterns such that the magnetic dipolar fields are repeated over a certain distance [7], [8]. Importantly, patterning of nanomagnets also allows control over the dynamic magnetic excitations, or spin waves, opening the possibility to coherently control spin qubits at the low power consumption [9] limit, characteristic to spintronic and magnonic devices [10]. Spin waves can propagate over distances up to several millimeters [11], can be steered [12], [13] and focused [10]. One application in particular would be the local amplification of microwave fields acting on the SiC spin centers using spin waves [9], [14], [15]. From a different standpoint, spin qubits can be used to sense magnetic excitations with high spatial resolution [16], [17]. For instance, this would allow the search for radiating microwave fields in spin orbit torque based nano-oscillators [18], [19]. In order to achieve such hybrid magnon-quantum systems associated with dynamic dipolar fields, it is very important to first understand the effect of static magnetic dipolar fields, which is the subject of this letter.

Corresponding author: F. J. T. Goncalves (f.goncalves@hzdr.de)

Though SiC is a natural material of choice for the aforementioned hybrid quantum platform at the wafer scale [20], [21], most of the efforts are put so far on the NV centers in diamond [1], [3], [5], [9], [16], [17].

In this letter, we demonstrate the use of spin centers created by proton irradiation in SiC as sensors for the static in-plane magnetic dipolar fields surrounding a magnetic nanostructure. Homogeneous proton irradiation was done such that a high density of spin color centers was bound to the surface closest to the magnetic element to ensure optimal sensitivity. The spin resonance of these centers was driven by a patterned micrometer-sized microwave antenna such that the microwave signal is delivered locally and confined to the region of interest. Compared to conventional millimeter-sized microwave circuits, the patterned antennas were found to be more efficient at driving the resonance of the spin centers due to the scaling of the circuit dimensions. We find that the spatial profile of the magnetic dipolar fields produced by the magnetic element varies with the applied field direction and the magnetic state.

II. Sample Characterisation and Methods

We perform proton irradiation on a high purity semi-insulating 4H-SiC single crystal with a fluence of 10^{15} cm^{-2} [22]. The energy of the irradiated protons was 30 keV and corresponds to a mean projected range of 200 nm below the surface. The optically active spin centers are excited with a 785 nm laser and the detected photoluminescence (PL) in the spectral range from $850\,\mathrm{nm}$ to $1050\,\mathrm{nm}$ is characteristic for the V_{Si} centers in SiC [23]. After proton irradiation, the SiC substrate went through two electron beam lithography (EBL) steps that enabled the fabrication of the micrometer-sized microwave circuit and the magnetic element. The microwave circuit consists of sputtered Cr (6 nm)/Au (150 nm) layers

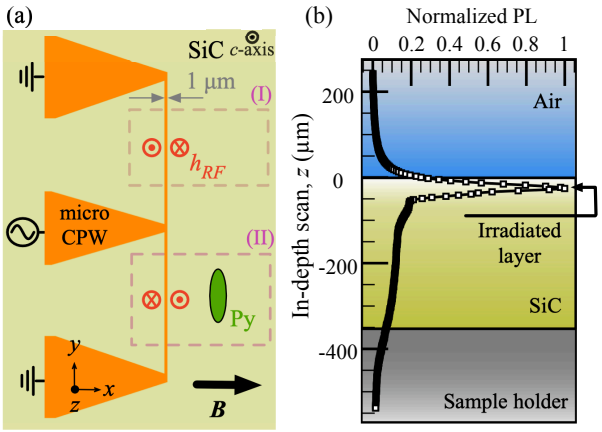

Fig. 1. (a) Schematic illustration of the micro-CPW and the magnetic element (Py) fabricated on the SiC substrate. The symbols labelled as h_{RF} illustrate the out-of-plane direction of the microwave fields. Both the micro-CPW and the magnetic element were patterned on the surface closest to the proton-irradiated SiC layer. The magnetic element is a 8 µm × 2 µm ellipse. (b) In-depth scan of the PL (normalised) across the SiC substrate measured in region (I).

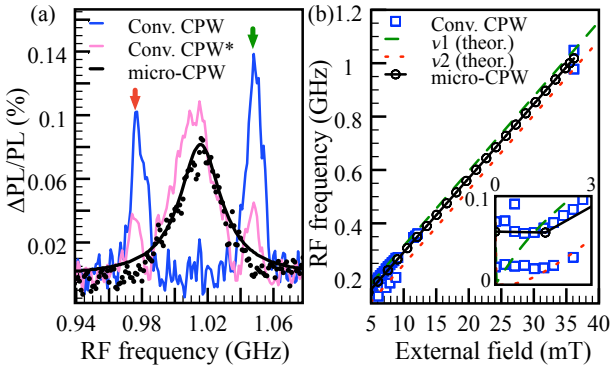

Fig. 2. (a) ODMR spectrum of: the proton-irradiated layer in SiC (black) obtained using the micro-CPW; the pristine SiC bulk substrate (blue) measured using the conventional CPW; both proton irradiated and bulk SiC obtained using the conventional CPW while the substrate was in a flip-chip configuration. The data was acquired at room temperature at an external magnetic field of 36 mT. (b) Field dependence of the ODMR frequency peak obtained following a Lorentzian fit to the experimental data. The averaged error in fitting the resonances was 0.5 MHz. The dashed lines ν_1 and ν_2 show the spin resonance frequencies which are solutions to the effective Hamiltonian of spin-3/2 centers in SiC, for in-plane magnetic fields, in the pristine SiC crystal [25]. The inset plot shows the near-zero field region where the ODMR peaks were observed at 60 MHz (micro-CPW), 20 MHz and 71 MHz (conventional CPW).

and the geometry corresponds to that of a shorted co-planar waveguide antenna (micro-CPW) as illustrated in Fig. 1(a). The magnetic element is a 8 µm × 2 µm ellipse consisting of 50 nm thick $Ni_{81}Fe_{19}$ (Py). In the schematic of Fig. 1(a), we highlight two regions of the micro-CPW: region (I), where there is no influence from the magnetic element; and region (II), where the ellipse was patterned such that the effect of the magnetic dipolar fields could be probed. A separation of 40 µm between the two regions ensured that region (I) did not experience any magnetic dipolar fields originating from the magnetic element. It is important to note that the efficiency and direction of the microwave excitation field is the same at both regions (I) and (II). Considering the lateral position of the microwave circuit with regard to the probed regions and the close proximity in height to the proton-irradiated SiC layer, one expects the microwave fields to be predominantly in the out-of-plane direction.

Figure 1(b) shows an in-depth PL scan across the substrate, measured in region (I). Here, one can see that the proton-irradiated layer yields a considerably larger PL. On all experiments carried out, the z-position of the objective focal plane was chosen such that PL acquisition was maximised. The PL was acquired using a Si avalanche photodetector (Thorlabs APD440A) connected to a lock-in amplifier whose modulation frequency was set via amplitude modulation of the probing laser. In order to enhance the spatial resolution, a spatial filter with a 30 µm pinhole was added to the detection path such that the measured PL originated only from a fraction of the volume illuminated by the incident laser. Thus, allowing spatial scans with a resolution of 1.30 µm, 1.65 µm and 28 µm in the x, y and z directions, respectively.

Optically detected magnetic resonance (ODMR) [2] was employed to measure the intrinsic resonance properties of the spin centers in region (I) as well as the effect of the magnetic element in region (II). This method is based on the relative change of the PL intensity, $\Delta\mathrm{PL}/\mathrm{PL}$, under spin resonance conditions [2] (i.e. driven by external microwave signals). In this particular measurement setup, the ODMR spectra were obtained via the same lock-in detection method as the PL, except that the microwave signal was modulated instead of the laser. The main focus of our experiments was the limit of strong magnetic fields $\gamma B \gg 2D$. Here, γ is the gyromagnetic ratio for the electrons captured by the V_{Si} centers and $2D$ is a zero field splitting in the V_{Si} centers. In 4H-SiC, the latter can take the values $4.5\,\mathrm{MHz}$ or $70\,\mathrm{MHz}$, depending on the crystallographic configuration [2], [24]. For $|\gamma| = 28\ \mathrm{MHz/mT}$ which is the same as for an isolated electron, the above condition of the strong magnetic field is fulfilled for $B \gg 2.5\,\mathrm{mT}$. In this limit the spin resonance frequencies shift linearly with B following $\nu_{1,2} = \gamma B \pm D(3\cos^2\theta - 1)$ [25], [26]. The splitting between two spin resonances $\nu_1 - \nu_2$ depends on the angle θ between the magnetic field and the symmetry axis of the spin center. For the case of pristine samples, the symmetry axis is parallel to the c-axis of the 4H-SiC lattice. In the context of the present experiments, the static magnetic field is applied perpendicular to the c-axis and the driving microwave field is applied parallel to the c-axis.

III. Experimental Results and Discussion

Figure 2(a) shows the ODMR spectra of the proton-irradiated SiC layer obtained using the micro-CPW as the source for the driving microwave fields, at a constant in-plane field of 36 mT. The output power of the microwave source was set to 4 dBm and the electrical contact with the micro-CPW was done using a ground-signal-ground (GSG) probe. The resulting spectrum, shown in black (markers and Lorentzian fitting curve), exhibits one resonance peak at 1.018 GHz with a linewidth of 37.0 ± 0.5 MHz. As a control measurement,

we acquired the ODMR spectrum originating from the bulk of the SiC substrate using a commercially available CPW with a signal line width of 275 µm as the source of the driving microwave fields. On this particular experiment, the output power of the microwave source had to be increased to 25 dBm in order to obtain an ODMR amplitude comparable to that obtained using the micro-CPW. The corresponding spectrum is also shown in Fig. 2(a) (blue) and exhibits two resonance peaks at 0.978 GHz and 1.048 GHz, with linewidths of 13 MHz. The spectra acquired using these two different excitation methods should have yielded similar results but clearly differ in both the number of peaks and the frequency linewidth. In order to understand the difference between these two spectra we present a third ODMR spectrum which was obtained from the same region of the substrate using the conventional CPW as the source of the microwave driving fields, except this time the substrate was positioned in a flip-chip configuration. This configuration allowed to achieve the shortest possible distance between the proton-irradiated SiC layer and the conventional CPW, ultimately resulting in stronger driving microwave fields. This ODMR spectrum (magenta line in Fig. 2(a)) revealed three resonance peaks, the two side peaks appear to coincide with those originating from the bulk of the SiC substrate, while the broader centre peak coincides with that of the proton-irradiated SiC layer. This result suggests that the difference in lineshape is caused by the proton irradiation fluence chosen for this particular SiC substrate.

Intense proton irradiation leads to inhomogeneous broadening due to local changes in the crystalline environment around each V_{Si} center [27], [28]. Both, the $2D$ zero-field splitting and the orientation of the symmetry axis can be affected. As a consequence, a broad resonance peak is observed instead of the double peak structure characteristic of the pristine SiC crystal. Nevertheless, the single ODMR resonance observed shifts linearly with magnetic field applied perpendicular to the c-axis as shown by the field dependence plotted in Fig. 2(b). From the fit of the experimental data we obtained a slope of 27.4 ± 0.2 MHz/mT. This value is close to the gyromagnetic ratio of an isolated electron and also very similar to that observed for the two resonance peaks originating from the bulk SiC crystal. A more detailed discussion on the effect of the irradiation fluence on the ODMR spectra of SiC will be discussed elsewhere. Having identified the characteristic ODMR spectra of the proton-irradiated SiC layer, we proceed to demonstrate the spatial mapping of the magnetic dipolar fields produced by the magnetic element in region (II).

Figure 3(a) shows the ODMR spectra measured at various y-positions along the longest axis of the magnetic element[1]. The scanning line was parallel to the micro-CPW, as illustrated on the schematic on the left (dashed red line). This way,

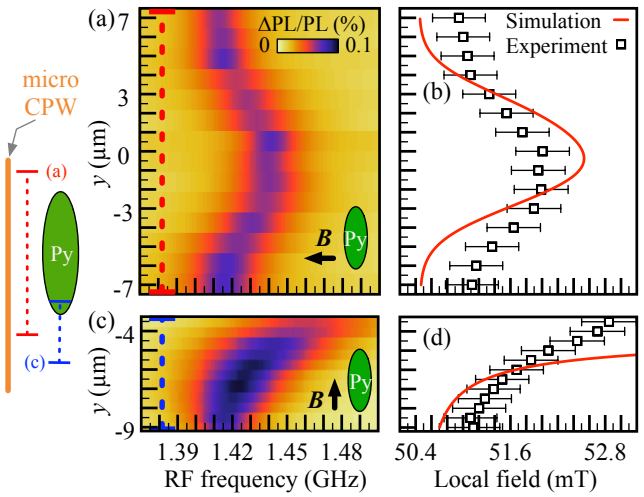

Fig. 3. (a) ODMR spectra acquired at various positions parallel to the long axis of the ellipse. The scan indicated by the red dashed line was located 4 µm from the edge of the micro-CPW and 2 µm from the edge of the ellipse. A magnetic field of 50.5 mT was applied in-plane, as illustrated in the inset schematic. (b) Plot of the in-plane magnetic dipolar fields obtained from the simulations (line) and the in-plane magnetic field converted from the ODMR frequency shifts (markers). (c) ODMR spectra acquired at various positions collinear with the long axis of the ellipse (see inset schematic on the left). The scan line (blue dashed line) was located 7 µm from the edge of the micro-CPW. The in-plane magnetic field (50.5 mT) was applied parallel to the long axis of the ellipse. (d) Comparison between the local in-plane magnetic field converted from the ODMR frequency shifts and the in-plane magnetic dipolar fields obtained from the simulations. Error bars in (b) and (d) show the fitting errors converted to units of millitesla.

we ensured constant microwave excitation efficiency at the probed positions. Here, an in-plane magnetic field of 50.5 mT was applied perpendicular to the long axis of the magnetic element and the microwave power was set to 0 dBm. At the outer positions of the ellipse ($\pm$ 7 µm) the ODMR frequency is 1.412 GHz and increases towards 1.442 GHz as the shortest distance to the ellipse is reached (y= 0). This frequency shift is a direct consequence of the magnetic dipolar field distribution generated by the magnetic element. Taking into consideration the fitting parameters obtained from the data shown in Fig. 2(b), we converted the ODMR frequency shifts to local fields, as plotted in Fig. 3(b). The local field accounts for the external field and the magnetic dipolar field contribution, amounting to 52.0 mT near y= 0 and 50.9 mT in the outer positions ($\pm$ 7 µm) where the magnetic dipolar field contribution is very small. On this same plot, we included the magnetic dipolar field distribution obtained via micromagnetic simulations (using Mumax3 [29]), for this particular sample geometry[2]. At an applied field of 50.5 mT, the magnetic ground state of the ellipse is practically saturated along the field direction. Note that the spatial variation of the magnetic dipolar field obtained from the simulation is in good agreement with that obtained from the experiments. We stress that the discrepancy does not exceed 0.6 mT or 1% with respect to the magnetic field strength. The difference in absolute numbers, between the simulations and the experimental data, may be due

[1]For easier visualisation, the data presented in the color plots of Figs.3(a),(c) and 4(a) correspond to fitted Lorentzian functions (each frequency spectrum was smoothed and fitted using a Lorentzian lineshape)of the raw data. The fitting errors were very small compared to the measured quantities, justifying our approach. The average fitting errors in were: 3(a) frequency peak 0.5 MHz, peak amplitude 10^{-3}, FWHM 2 MHz.; 3(c) frequency peak 0.3 MHz, peak amplitude 10^{-5}, FWHM 0.3 MHz; 4(a) frequency peak 0.4 MHz, peak amplitude 10^{-3}, FWHM 0.7 MHz.

[2]Simulation size: 20 µm by 14 µm by 50 nm and magnetic parameters used: M_s= 810 kA/m, A_{ex}= 13 pJ/m, damping α= 0.007, γ= 29.6 GHz/T

to deviations from the actual saturation magnetisation and the fact that edge roughness was not considered in the simulations.

Consider the scenario where the external magnetic field is applied parallel to the long axis of the ellipse. This case is discussed in Fig. 3(c), where the ODMR spectra are plotted as a function of the distance to the pole of the ellipse (see illustration on the left). In this experiment the microwave power was increased to 13 dBm to compensate for the weaker driving fields due to a larger distance to the micro-CPW. The ODMR frequency appears to follow a near asymptotic behaviour as the ellipse is approached, which highlights the possibility to achieve very strong local magnetic fields near the edges of the magnetic element. The increase in the resonance linewidth from 30 MHz (y= -5 µm) to 67 MHz (y= -0.5 µm) can be explained by the larger magnetic dipolar fields when probing closer to edge of the magnetic element. The reduction in the ODMR amplitude near the edge of the ellipse (y= 0) is due to the partial overlap between the probing laser beam and the magnetic material. Moreover, we expect that the lateral resolution (~ 1.65 µm), imposed by the size of the PL acquisition volume, also affects the agreement with the magnetic dipolar field profiles shown in Figs. 3(b) and (d). Improvements should be made in terms of spatial resolution in order to increase the field sensitivity beyond the sub-millitesla limit which is currently achieved [1], [5].

In order to further demonstrate the degree of localisation achieved using the lithographically defined micro-CPW and magnetic elements in combination with the proton-irradiated layer, we performed a control experiment where we mapped the magnetic dipolar fields of the ellipse using the conventional CPW, in a flip-chip configuration. The layout of this experiment is shown in Fig. 4(a). We note that the magnetic element was placed in the gap between the ground and the signal line of the CPW which means that the driving microwave fields are predominantly oriented out-of-plane, as in the case of the micro-CPW. The spatial mapping of the ODMR spectra is shown in Fig. 4(a). Similarly to the data shown in Fig. 2(a) (magenta line), we observe two side resonance peaks and a broader center resonance peak. Importantly, note that only the center peak shifts in frequency when varying the y-position. This means that while the SiC spin centers are being uniformly excited across the depth by the driving microwave fields, only the irradiated layer in close proximity to the ellipse is sensing the magnetic dipolar fields. The two side resonance peaks arising from the bulk are insensitive to the local magnetic dipolar fields and can be used to independently measure the external magnetic field.

Figure 4(b) shows the ODMR spectra acquired at y= 7 µm (blue) and 0 µm (red) positions of the scan line. The difference in ODMR peak position between these two modes yielded the largest frequency shift observed in this experiment (14 MHz). This value differs from that observed using the micro-CPW (30 MHz, see Fig. 3) due to loss of spatial resolution as the spatial filter was removed from the detection in this experiment. Another consequence of removing the spatial filter is that the PL acquisition depth was greatly increased. The loss in resolution and the fact that there are local changes in the refractive index due to the proximity to the magnetic element

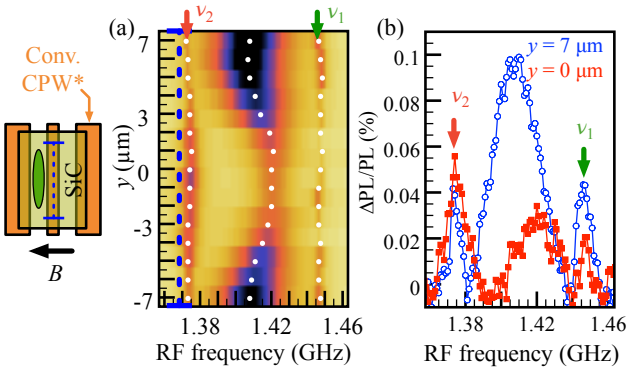

Fig. 4. (a) ODMR spectra acquired at various positions along the longest axis of the ellipse, as illustrated by the blue dashed line shown in the schematic on the left. White markers correspond to Lorentzian fits to the experimental data. The maximum value of the contrast is set to a $\Delta\mathrm{PL}/\mathrm{PL}$ value 0.08%. (b) Examples of the ODMR lineshape obtained from (a) for y= 7 µm and y= 0 µm. The narrow satellite peaks have approximately the same frequency as those expected for ν_1 and ν_2, shown in Fig. 2(b).

(effectively a metal/SiC interface, as opposed to an air/SiC interface), could explain the amplitude variation of the ODMR signal from the irradiated layer and the bulk. Importantly, it is worth noting that in order to detect the ODMR spectra shown here, the microwave input power had to be increased to 25 dBm, which is larger than that used in the micro-CPW measurements, by a factor of 315.

IV. Conclusion

In conclusion, we utilised SiC spin centers as sensors for the magnetic dipolar fields generated by a lithographically defined magnetic microstructure. The two magnetic states we investigated generate a distinct spatial distribution of the ODMR spectra, highlighting that both the shape of the magnetic element and the applied field direction can be used to locally modify the resonance of the spin centers in SiC. The integration of the microwave circuit contributed to an increase in ODMR sensitivity compared to the use of millimeter-sized CPWs due to a more efficient and localised delivery of microwave signal driving the resonance of the spin centers.

The results obtained here may be seen as a first step toward utilizing our antenna configuration to excite magnetization dynamics inside the micromagnet and study how the dynamic dipolar fields created can interact with the spin centers in the SiC crystal.

Acknowledgments

We thank Lukas Körber and Attila Kákay for their support and useful discussions related to micromagnetic simulations. This work was supported by the German Research Foundation (DFG) under the grants SCHU 2922/4-1 and AS 310/5-1. The lithography was done at the Nanofabrication Facilities (NanoFaRo) at the Institute of Ion Beam Physics and Materials Research, HZDR. Support from the Ion Beam Center (IBC) at Helmholtz-Zentrum Dresden-Rossendorf (HZDR) is gratefully acknowledged for the proton irradiation.

REFERENCES

[1] C. L. Degen, "Scanning magnetic field microscope with a diamond single-spin sensor," *Applied Physics Letters*, vol. 92, no. 24, p. 243111, jun 2008. [Online]. Available: http://aip.scitation.org/doi/10.1063/1.2943282

[2] H. Kraus, V. A. Soltamov, F. Fuchs, D. Simin, A. Sperlich, P. G. Baranov, G. V. Astakhov, and V. Dyakonov, "Magnetic field and temperature sensing with atomic-scale spin defects in silicon carbide," *Scientific Reports*, vol. 4, no. 1, p. 5303, may 2015. [Online]. Available: http://www.nature.com/articles/srep05303

[3] G. Balasubramanian, P. Neumann, D. Twitchen, M. Markham, R. Kolesov, N. Mizuochi, J. Isoya, J. Achard, J. Beck, J. Tissler, V. Jacques, P. R. Hemmer, F. Jelezko, and J. Wrachtrup, "Ultralong spin coherence time in isotopically engineered diamond," *Nature Materials*, vol. 8, no. 5, pp. 383–387, may 2009. [Online]. Available: http://www.nature.com/articles/nmat2420

[4] D. Simin, H. Kraus, A. Sperlich, T. Ohshima, G. V. Astakhov, and V. Dyakonov, "Locking of electron spin coherence above 20 ms in natural silicon carbide," *Physical Review B*, vol. 95, no. 16, p. 161201, apr 2017. [Online]. Available: http://link.aps.org/doi/10.1103/PhysRevB.95.161201

[5] G. Balasubramanian, I. Y. Chan, R. Kolesov, M. Al-Hmoud, J. Tisler, C. Shin, C. Kim, A. Wojcik, P. R. Hemmer, A. Krueger, T. Hanke, A. Leitenstorfer, R. Bratschitsch, F. Jelezko, and J. Wrachtrup, "Nanoscale imaging magnetometry with diamond spins under ambient conditions," *Nature*, vol. 455, no. 7213, pp. 648–651, oct 2008. [Online]. Available: http://www.nature.com/articles/nature07278

[6] D. Simin, V. A. Soltamov, A. V. Poshakinskiy, A. N. Anisimov, R. A. Babunts, D. O. Tolmachev, E. N. Mokhov, M. Trupke, S. A. Tarasenko, A. Sperlich, P. G. Baranov, V. Dyakonov, and G. V. Astakhov, "All-Optical dc Nanotesla Magnetometry Using Silicon Vacancy Fine Structure in Isotopically Purified Silicon Carbide," *Physical Review X*, vol. 6, no. 3, p. 031014, jul 2016. [Online]. Available: https://link.aps.org/doi/10.1103/PhysRevX.6.031014

[7] C. S. Davies, A. V. Sadovnikov, S. V. Grishin, Y. P. Sharaevskii, S. A. Nikitov, and V. V. Kruglyak, "Generation of propagating spin waves from regions of increased dynamic demagnetising field near magnetic antidots," *Applied Physics Letters*, vol. 107, no. 16, p. 162401, 2015. [Online]. Available: http://dx.doi.org/10.1063/1.4933263

[8] Y. Li, G. Gubbiotti, F. Casoli, S. A. Morley, F. J. T. Gonçalves, M. C. Rosamond, E. H. Linfield, C. H. Marrows, S. McVitie, and R. L. Stamps, "Thickness dependence of spin wave excitations in an artificial square spin ice-like geometry," *Journal of Applied Physics*, vol. 121, no. 10, p. 103903, mar 2017. [Online]. Available: http://aip.scitation.org/doi/10.1063/1.4978315

[9] P. Andrich, C. F. de las Casas, X. Liu, H. L. Bretscher, J. R. Berman, F. J. Heremans, P. F. Nealey, and D. D. Awschalom, "Long-range spin wave mediated control of defect qubits in nanodiamonds," *npj Quantum Information*, vol. 3, no. 1, p. 28, dec 2017. [Online]. Available: http://www.nature.com/articles/s41534-017-0029-z

[10] A. Hoffmann and H. Schultheiß, "Mesoscale magnetism," *Current Opinion in Solid State and Materials Science*, vol. 19, no. 4, pp. 253–263, 2015. [Online]. Available: http://linkinghub.elsevier.com/retrieve/pii/S1359028614000874

[11] L. Flacke, L. Liensberger, M. Althammer, H. Huebl, S. Geprägs, K. Schultheiss, A. Buzdakov, T. Hula, H. Schultheiss, E. R. J. Edwards, H. T. Nembach, J. M. Shaw, R. Gross, and M. Weiler, "High spin-wave propagation length consistent with low damping in a metallic ferromagnet," *Applied Physics Letters*, vol. 115, no. 12, p. 122402, sep 2019. [Online]. Available: http://aip.scitation.org/doi/10.1063/1.5102132

[12] K. Vogt, F. Fradin, J. Pearson, T. Sebastian, S. Bader, B. Hillebrands, A. Hoffmann, and H. Schultheiss, "Realization of a spin-wave multiplexer," *Nature Communications*, vol. 5, no. 1, p. 3727, sep 2014. [Online]. Available: http://www.nature.com/articles/ncomms4727

[13] K. Wagner, A. Kákay, K. Schultheiss, A. Henschke, T. Sebastian, and H. Schultheiss, "Magnetic domain walls as reconfigurable spin-wave nanochannels," *Nature Nanotechnology*, vol. 11, no. 5, pp. 432–436, may 2016. [Online]. Available: http://dx.doi.org/10.1038/nnano.2015.339

[14] D. Kikuchi, D. Prananto, K. Hayashi, A. Laraoui, N. Mizuochi, M. Hatano, E. Saitoh, Y. Kim, C. A. Meriles, and T. An, "Long-distance excitation of nitrogen-vacancy centers in diamond via surface spin waves," *Applied Physics Express*, vol. 10, no. 10, p. 103004, oct 2017. [Online]. Available: https://iopscience.iop.org/article/10.7567/APEX.10.103004

[15] E. Lee-Wong, R. Xue, F. Ye, A. Kreisel, T. van der Sar, A. Yacoby, and C. R. Du, "Nanoscale Detection of Magnon Excitations with Variable Wavevectors Through a Quantum Spin Sensor," *Nano Letters*, vol. 20, no. 5, pp. 3284–3290, may 2020.

[16] S. Steinert, F. Dolde, P. Neumann, A. Aird, B. Naydenov, G. Balasubramanian, F. Jelezko, and J. Wrachtrup, "High sensitivity magnetic imaging using an array of spins in diamond," *Review of Scientific Instruments*, vol. 81, no. 4, p. 043705, apr 2010. [Online]. Available: http://aip.scitation.org/doi/10.1063/1.3385689

[17] L. Rondin, J. P. Tetienne, S. Rohart, A. Thiaville, T. Hingant, P. Spinicelli, J. F. Roch, and V. Jacques, "Stray-field imaging of magnetic vortices with a single diamond spin," *Nature Communications*, vol. 4, no. 1, p. 2279, oct 2013. [Online]. Available: http://www.nature.com/articles/ncomms3279

[18] B. Divinskiy, V. E. Demidov, S. Urazhdin, R. Freeman, A. B. Rinkevich, and S. O. Demokritov, "Excitation and Amplification of Spin Waves by Spin-Orbit Torque," *Advanced Materials*, vol. 30, no. 33, p. 1802837, aug 2018. [Online]. Available: http://doi.wiley.com/10.1002/adma.201802837

[19] T. Hache, Y. Li, T. Weinhold, B. Scheumann, F. J. T. Gonçalves, O. Hellwig, J. Fassbender, and H. Schultheiss, "Bipolar spin Hall nano-oscillators," *Applied Physics Letters*, vol. 116, no. 19, p. 192405, may 2020. [Online]. Available: http://aip.scitation.org/doi/10.1063/5.0008988

[20] S. Castelletto and A. Boretti, "Silicon carbide color centers for quantum applications," *Journal of Physics: Photonics*, vol. 2, no. 2, p. 022001, mar 2020. [Online]. Available: https://iopscience.iop.org/article/10.1088/2515-7647/ab77a2

[21] N. T. Son, C. P. Anderson, A. Bourassa, K. C. Miao, C. Babin, M. Widmann, M. Niethammer, J. Ul Hassan, N. Morioka, I. G. Ivanov, F. Kaiser, J. Wrachtrup, and D. D. Awschalom, "Developing silicon carbide for quantum spintronics," *Applied Physics Letters*, vol. 116, no. 19, p. 190501, may 2020. [Online]. Available: http://aip.scitation.org/doi/10.1063/5.0004454

[22] H. Kraus, D. Simin, C. Kasper, Y. Suda, S. Kawabata, W. Kada, T. Honda, Y. Hijikata, T. Ohshima, V. Dyakonov, and G. V. Astakhov, "Three-Dimensional Proton Beam Writing of Optically Active Coherent Vacancy Spins in Silicon Carbide," *Nano Letters*, vol. 17, no. 5, pp. 2865–2870, May 2017.

[23] D. Riedel, F. Fuchs, H. Kraus, S. Väth, A. Sperlich, V. Dyakonov, A. A. Soltamova, P. G. Baranov, V. A. Ilyin, and G. V. Astakhov, "Resonant Addressing and Manipulation of Silicon Vacancy Qubits in Silicon Carbide," *Physical Review Letters*, vol. 109, no. 22, p. 226402, nov 2012. [Online]. Available: https://link.aps.org/doi/10.1103/PhysRevLett.109.226402

[24] R. Nagy, M. Niethammer, M. Widmann, Y.-C. Chen, P. Udvarhelyi, C. Bonato, J. U. Hassan, R. Karhu, I. G. Ivanov, N. T. Son, J. R. Maze, T. Ohshima, Ö. O. Soykal, Á. Gali, S.-Y. Lee, F. Kaiser, and J. Wrachtrup, "High-fidelity spin and optical control of single silicon-vacancy centres in silicon carbide," *Nature Communications*, vol. 10, no. 1, p. 1954, dec 2019. [Online]. Available: http://www.nature.com/articles/s41467-019-09873-9

[25] H. Kraus, V. A. Soltamov, D. Riedel, S. Väth, F. Fuchs, A. Sperlich, P. G. Baranov, V. Dyakonov, and G. V. Astakhov, "Room-temperature quantum microwave emitters based on spin defects in silicon carbide," *Nature Physics*, vol. 10, no. 2, pp. 157–162, feb 2014. [Online]. Available: http://www.nature.com/articles/nphys2826

[26] D. Simin, F. Fuchs, H. Kraus, A. Sperlich, P. G. Baranov, G. V. Astakhov, and V. Dyakonov, "High-Precision Angle-Resolved Magnetometry with Uniaxial Quantum Centers in Silicon Carbide," *Physical Review Applied*, vol. 4, no. 1, p. 014009, jul 2015. [Online]. Available: https://link.aps.org/doi/10.1103/PhysRevApplied.4.014009

[27] C. Kasper, D. Klenkert, Z. Shang, D. Simin, A. Gottscholl, A. Sperlich, H. Kraus, C. Schneider, S. Zhou, M. Trupke, W. Kada, T. Ohshima, V. Dyakonov, and G. V. Astakhov, "Influence of Irradiation on Defect Spin Coherence in Silicon Carbide," *Physical Review Applied*, vol. 13, no. 4, p. 044054, apr 2020. [Online]. Available: https://link.aps.org/doi/10.1103/PhysRevApplied.13.044054

[28] A. Hernández-Mínguez, A. V. Poshakinskiy, M. Hollenbach, P. V. Santos, and G. V. Astakhov, "Anisotropic spin-acoustic resonance in silicon carbide at room temperature," *Phys. Rev. Lett.*, vol. 125, p. 107702, Sep 2020. [Online]. Available: https://link.aps.org/doi/10.1103/PhysRevLett.125.107702

[29] A. Vansteenkiste, J. Leliaert, M. Dvornik, M. Helsen, F. Garcia-Sanchez, and B. Van Waeyenberge, "The design and verification of MuMax3," *AIP Advances*, vol. 4, no. 10, p. 107133, oct 2014. [Online]. Available: http://aip.scitation.org/doi/10.1063/1.4899186